FINAL REPORT

Strong Ground Motions in Salt Lake City and Other Metropolitan Areas From Large Earthquakes on the Wasatch Fault

Award: G09AP00027
Start: January 1, 2009
End: December 31, 2010

Element II: Evaluate Urban Hazard and Risk

Ralph J. Archuleta

Earth Research Institute
University of California, Santa Barbara
Santa Barbara, CA 93106
Phone: 805 893-8441
Fax: 805 893-2578
Email: ralph@eri.ucsb.edu

Research supported by the U. S. Geological Survey (USGS), Department of Interior, under USGS award number G09AP00027. The views and conclusions contained in this document are those of the authors and should not be interpreted as necessarily representing the official policies, either expressed or implied, of the U. S. Government.

Abstract

We have computed ground motions from dynamic models of M 7 earthquakes on the Salt Lake City segment of the Wasatch Fault, Utah. The computations take into account the dip of the fault, the three-dimensional velocity structure and the dynamics of a spontaneously propagating rupture. The ground motions are limited to a maximum frequency of 1.0 Hz; we have limited the slowest shear wave velocity in the basin to 500 m/s. Thus one could expect larger ground motion amplification for the true velocity, which is more like 200-300 m/s. There are basin effects that prolong the duration and increase the amplitude of the ground motion. The largest ground motion amplitudes are near the trace of the Wasatch Fault caused by the breakout of the rupture at the surface. Peak offsets are on the order of 2 m, consistent with the paleoseismic data. The peak ground velocity on the footwall is consistent with the recently developed NGA relations; however, the NGA relations are larger than the computed peak ground velocity in the basin. This may be caused by our approximation of limiting the slowest shear wave speed to 500 m/s; a slower velocity would allow for more amplification of the ground motion. We approximated the Wasatch Fault on the Salt Lake City segment as 1) a single, dipping planar fault and as 2) a two-segment, sub-parallel, planar fault. The two-segment fault naturally produces a different ground motion from the single-segmented fault. However, until the rupture reaches the second segment, the ground motion is the same, as one would expect.

Strong Ground Motions in Salt Lake City and other Metropolitan Areas from Large Earthquakes on the Wasatch Fault

1. Background and Introduction

Approximately 80% of Utah's 2.7 million people live within 15 miles of the Wasatch Fault. This area is one of the most hazardous places in the US that under the threat of big earthquakes (Mw > 7). The Salt Lake City segment of the Wasatch Fault (SLCWF) poses a serious threat to the nearby city and surrounding communities. The SLCWF is a normal fault with a dip of about 50 degrees that forms a boundary between the Wasatch Mountains to the east and a relatively thin sedimentary basin to the west that rests on the hanging wall. Recently a 3D Wasatch Front Community Velocity Model (WFCVM) was released for the region.

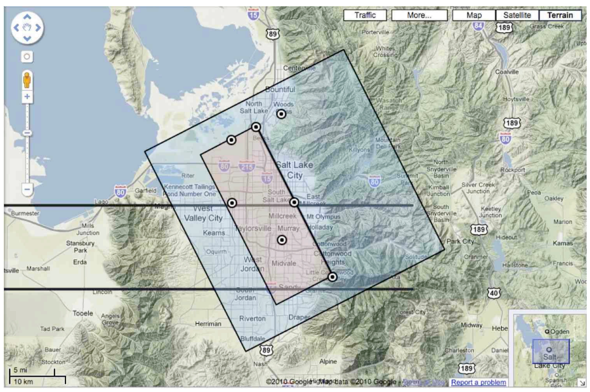

Figure 1: Map view of the modeling area. Blue square shows the computing area, red rectangle shows the projection of the planar fault plane

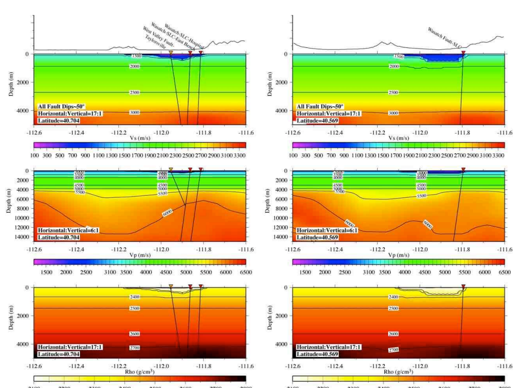

Figure 2: Cross-section profile of WFCVM under latitude of 40.504° and 40.569°, black line represents the fault, the vertical axis is exaggerated.

In Figure 2 we are showing the cross-section of velocity structures extracted from the WFCVM at certain latitude along longitude and depth. As the WFCVM shows, the sedimentary basin structure extends hundreds of kilometers wide to the west of the Wasatch Fault, while the thickness of the sediments is only 0.5km to 1km at most. This feature plays an important role in the basin effect. The basic property of the basin will determine the dominant frequency of reverberation. Also the low velocity in the basin determines the resolution of the numerical modeling.

2. Method

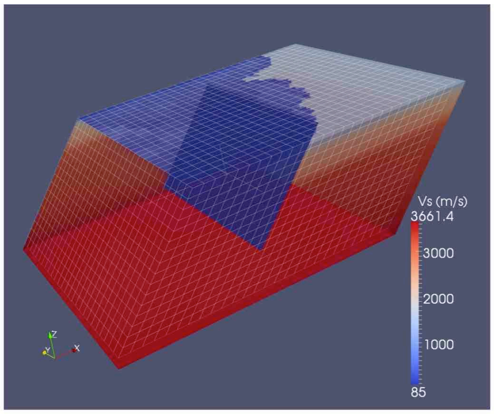

Figure 3: Finite Element meshing scheme of the problem, color coded by Vs, blue rectangular is the embedded planar fault plane.

To have a more accurate estimation of what the ground motion might be due to potential earthquakes (Mw. 7), we use a finite element method (Ma & Liu, 2006) to simulate dynamic ruptures on the fault embedded within the WFCVM.

We model the Salt Lake City segment as a planar fault, which extends to the free surface. Fault length along strike is 30km and fault width down-dip is 17.6km, with 50° dip angle. We extract the velocity structure information from the 3-D WFCVM and integrate it into our finite element model. We adapt the original velocity model by allowing Vs larger than 500m/s and Vp larger than 1500m/s, in consideration of our computation resolution. Figure 3 shows the meshing scheme of our modeling, color-coded by Vs.

We use homogeneous and heterogeneous initial stress condition in our simulations. For homogeneous initial stress configuration, we use 36MPa as the normal stress and 19.7MPa as the initial shear stress. We use 0.66 and 0.448 as static and dynamic friction coefficients, respectively. The major concern for this stress setting is that through the combination of values used here, we can get a stress drop of around 3.5MPa, which is the average stress drop for intraplate earthquakes observed around the globe. For heterogeneous initial stress configuration, we use the method by Lavallée et al. (2006) to construct the initial shear stress field. Normal stress is the same as in the homogeneous case thus uniform over the fault plane. The mean shear stress, static/dynamic friction coefficients are the same as in the homogeneous case. For any point on the fault, the fluctuation of the initial shear stress field follows a truncated Cauchy distribution. The correlation among different points on the fault satisfies a power law relation.

To initiate the rupture, we use a simple method by constructing a rectangular area with initial shear stress slightly above the local yield stress level. The hypocenter (initiation zone) is placed near the bottom of the fault plane.

We use slip-weakening friction law (Ida, 1972), with the Dc 0.25m. We don't have cohesion in the friction law. We allow changes of static and dynamic friction coefficient in different configurations of the problem. We put a strength barrier at the boundary of the fault except on the free surface side. In this way we prevent the rupture from propagating outside the predefined fault plane.

Lx, Ly, Lz	40 km, 40 km, 17 km
dx, dy, dz	50 m, 50 m, 50 m
Strike, dip angle	153°, 50°
Mean Slip, Magnitude	2.05 m, 6.9 M_w
Friction law	Slip weakening
Initial normal stress	36 MPa
μ0, μd, μs, S	0.55 (average), 0.448, 0.66, 1.1
Dc	0.25 m
Tmax	30 sec
Vs minimum	500 m/s
Maximum Freq	1 Hz

Table 1: Key parameters of simulations.

We add energy-absorbing layer (Scholz, 1998) near the free surface due to the concern of overwhelmingly large slip amplitude at shallow depth. We implemented the energy-absorbing layer by changing the dynamic friction coefficient from 0.448 to 0.55 in the first 2kms in our model, in order to emulate the velocity strengthening behavior. Here after we will call this special treated layer as V-S zone (Velocity Strengthening zone).

In Table 1, we provide typical values for the key parameters used in our simulations.

3. Results

Through the course of study, we investigated several important aspects, which might influence the ground motion prediction for the potential earthquake on SLCWF segment. We use the bulk material properties imported from WFCVM model and a regular meshing scheme. We change the initial stress condition and fault geometry to study the variation of the ground motion due to these uncertainties.

3.1 Planar fault without V-S zone

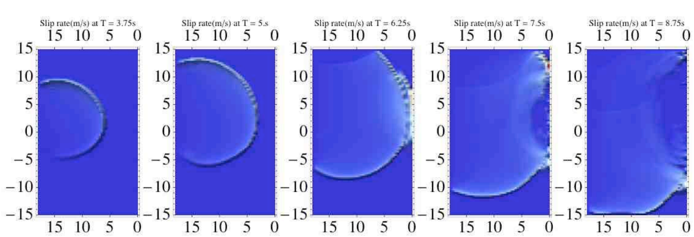

Figure 4: Snapshots of slip rate on the fault taken at 3.75s, 5.0 s, 6.25 s, 7.5 s and 8.75 s. This is for a dynamic rupture run with heterogeneous initial stress. Fault distance (km) along strike is vertical axis and along dip is horizontal axis.

We start from single planar fault with homogeneous and heterogeneous initial stress condition. We run around 20 simulations with different realizations of random initial stress conditions under the same statistical behavior. Figure 4 shows the rupture process snapshots from one run, which is a typical representative of the group of

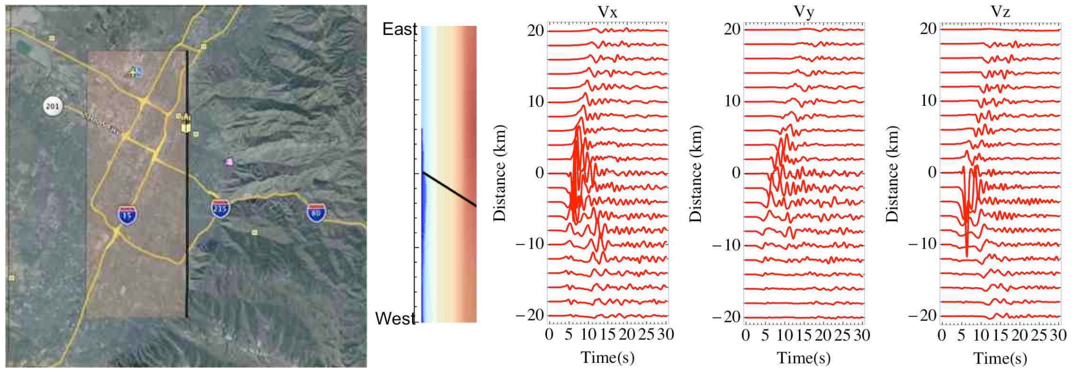

Figure 5: (left) map view of the modeling area, (middle) velocity structure under the red line, (right panel) 3 components of seismograms along the red line.

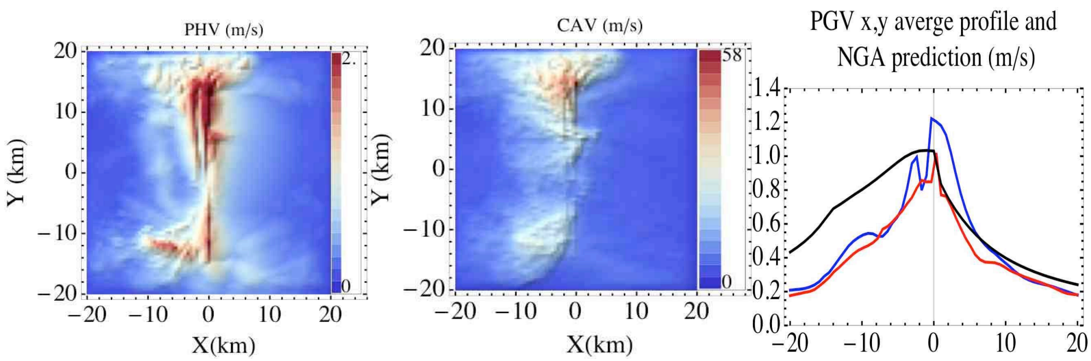

Figure 6: (left) PHV map for this simulation, (middle) CAV map, (right) averaged PGV-x, PGV-y and NGA prediction along X axis in blue, red and black curves respectively.

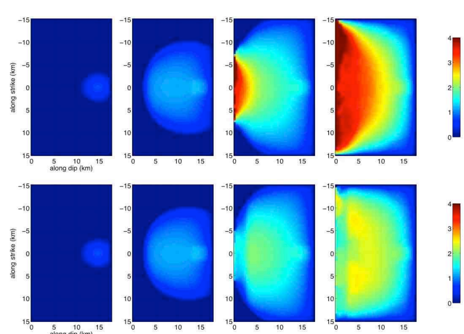

Figure 7: comparison of slip snapshots without (top) and with (bottom) V-S zone, snapshots taken at 1.9s, 5,6s, 7.5s, 10.0s

simulations. The rupture starts from the central bottom of the fault plane and propagate bilaterally. The asymmetry of the rupture front contour is due to the heterogeneity of the initial shear stress on the fault.

From Figure 5, we can see clearly of the basin effect. The signal tends to be amplified in the basin area and the duration tends to be longer. A long tail of reverberations is because the wave is trapped in the thin sediment basin.

In Figure 6, we plot the peak horizontal velocity (PHV) map as well as the cumulative absolute velocity (CAV) map here to show the general ground motion pattern. The area near the fault tip is under the most ground shaking. The velocity structure and the directivity effect both play important roles in determining the ground motion magnitude distribution. The averaged peak ground velocity is also plotted against the NGA prediction. It is obvious that on the hanging wall side the ground motion is over predicted while on the footwall side (hard rock) very near to the fault trace the ground motion is under predicted.

3.2 Planar fault with V-S zone

Geological observations show that the slip on the Wasatch Fault Salt Lake City segment is about 2m (DuRoss, 2008). But our preliminary simulations yield much larger slip at the shallow depth, which is against the data. To take this data into account, we implement an energy-absorbing layer in the shallow 2 km, which behaves in a velocity strengthening way. Figure 7 shows the difference of rupture process due to the V-S zone. The comparison is done under the same homogeneous initial stress configuration. We can tell from Figure 7 that the difference starts to show up when it ruptures to the free surface. With the help of Velocity Strengthening zone, the total slip near the free surface is significantly reduced, to around 2.5m, consistent with the paleoseismology results (DuRoss, 2008). The magnitude of the earthquake is reevaluated to be Mw 6.8, a little less than Mw.6.9 of the one without V-S zone. The corresponding ground motion is also reduced, especially in the area near the fault trace (Figure 8).

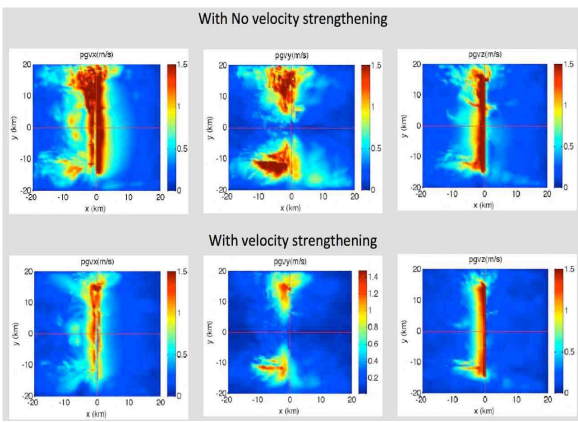

Figure 8: Comparison of 3 component PGV map between without V-S zone and with V-S zone, all of setting up are the same

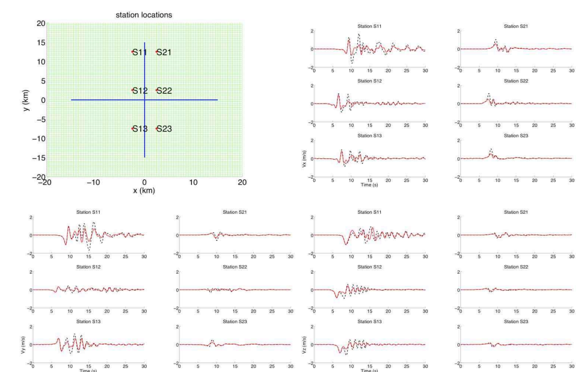

Figure 9: Comparison of seismograms without (black) and with (red) V-S zone. The location of the stations are shown in the top left corner.

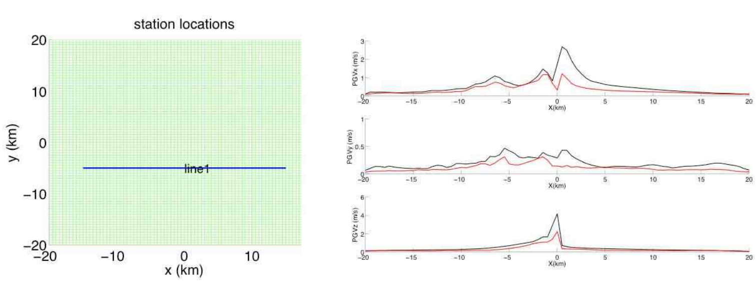

Figure 10: Comparison of 3 components of PGV profile without (black) and with (red) V-S zone, along the blue line shown on the left.

By inspecting the details of the seismogram (Figure 9), we are able to tell the role of the V-S zone on the ground motion. The V-S zone kills the second pulses, acting as a damper. The effect is most significant near the fault trace, but as we go farther away from the fault, the influence of the V-S zone on the ground motion becomes less (Figure 10). If we look at the ground motion statistics between the two settings, we can see the influence of the V-S zone more or less localize near the fault plane, reducing more than 50% of peak velocity in this case run.

Figure 11: Mapped SLCWF fault trace (red). It can be approximated by 4 segments (cyan).

3.2 Two-segment fault with V-S zone

Faults are not single planar features but complex in shape, connectivity, etc (Sibson 1989, Wesnousky 2006). Fault jumping and dynamic triggering can significantly change the seismic moment, therefore seismic hazard. Up to now, there are only limited quantitative investigations on how dynamic triggering occurs. In the previous sections, we simplify the Wasatch Fault Salt Lake City segment as a single planar normal fault. To depict the details of the bending and corners of this segment, one can have a more complex fault geometry model (Figure 11). Whether the potential earthquake can jump between adjacent segments (sections) and how would the hazard map change accordingly is the question we want to explore. Here we are giving some preliminary results on related questions.

Keyword	Value
Lx, Ly, Lz	40km,40km,17km
dx,dy,dz	100m,100m,100m
Strike,dip	180°, 50°
Friction Law	Slip-weakening
Initial normal stress	• Uniform (36MPa) • Depth dependent
μ_0, μ_d, μ_s, S	0.549 (0.546), 0.448, 0.66, 1.1 (1.16)
D_c	0.25m
dt, Tmax	0.01, 20.0
V_p, V_s, ρ	5.7km/s, 3.3km/s, 2700kg/m^3
Cohesion	0

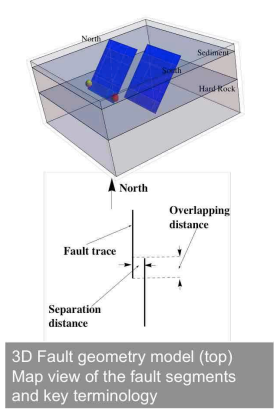

Figure 12: Geometry and parameters of the multi-segment dynamic simulation.

We split the previous 30km long single fault to two parallel segments of 18km and 12km (Figure 12). We change the overlapping and separation distance of the two segments to study under what geometric condition could the rupture jump between segments. Our results show that, under the simple assumptions of initial shear stress conditions as we used in single fault simulations, the rupture can jump if the separation distance is below 1.5 km.

Our results also show that hypocenter location plays an important role in multi-segment simulations. In one simulation, we put the hypocenter in the north of the first segment and the earthquake ruptures through the two segments. But if we put the hypocenter in the south of the first segment (nearer to the overlap of two segments) then the rupture is not able to continue on the second segment. The hypocenter location controls the rupture directivity, thus in some situation determines if there's enough energy for the rupture to jump between adjacent segments.

Through the comparison of single fault and two-segment fault cases, we see that it can generate quite different patterns of results in terms of slip distribution on fault as well as ground motion statistics. Figure 13 shows the slip snapshots on the fault. We can see that both models nucleate at the bottom corner in the north of the fault. The results start to differentiate when the rupture was slowed down by the separation of the segments. The maximum total slip is reduced in the two-segment case because of the slow down of the rupture speed. The severity of ground motion is influenced accordingly as shown in Figure 14.

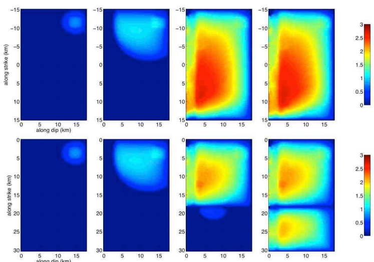

Figure 13: Comparison of snapshots of slip on the fault taken at 1.9s, 5.6s, 13.0s, 20.0s. The top shows the single fault and bottom the two-segment model.

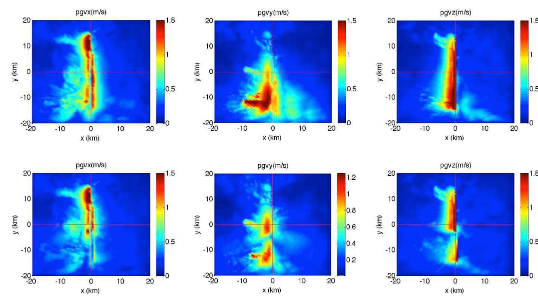

Figure 14: Comparison of surface PGV (root mean square of all 3 components) for a single fault (top) and a two-segment (bottom) fault.

4. Conclusion and Discussion

We model the dynamic rupture process of a potential Mw. 7 earthquake on the Wasatch Fault Salt Lake City segment using a finite element method. We import the 3-D velocity structure from the current Wasatch Front Community Velocity Model. We assign both homogeneous and heterogeneous initial shear stress in our simulations. Homogeneous initial stress is set up so that the expected stress drop is around 3.5MPa, which is in the range of global average stress drop for intraplate earthquakes. Heterogeneous initial shear stress is set up so that the one-point statistics follows a Gaussian distribution and two-point statistics follows a truncated Cauchy distribution. We found that a velocity-strengthening zone is important in order to get reasonable slip near the surface compatible to the observation. To investigate the effect of complex fault geometry, we further model the fault segment as a two-section fault. We find that segmentation of the fault will have significant influence on the rupture process as well as the ground motion statistics. A 1.5km separation threshold is estimated under the preliminary model for the rupture to jump between segments.

References:

DuRoss, C. B. (2008) Holocene vertical displacement on the central segments of the Wasatch Fault Zone, Utah, *Bulletin Seismological Society of America 98*, 2918-2933.

Ida, Y. (1972) Cohesive force across the tip of a longitudinal-shear crack and Griffith's specific surface energy. *Journal of Geophysical Research* 77, 3796--3805.

Lavallée, D., Liu, P., & Archuleta, R. J. (2006) Stochastic model of heterogeneity in earthquake slip spatial distributions. *Geophysical Journal International* 165, 622--640.

Ma, S. & Liu, P. (2006) Modeling of the perfectly matched layer absorbing boundaries and intrinsic attenuation in explicit finite-element methods. *Bulletin of the Seismological Society of America* 96, 1779.

Scholz, C. H. (1998) Earthquakes and friction laws. *Nature* 391, 37--42.

Sibson, R. H. (1989) Earthquake faulting as a structural process. *Journal of Structural Geology* 11, 1--14.

Wesnousky, S. G. (2006) Predicting the endpoints of earthquake ruptures. *Nature* 444, 358--360.

Bibliography of Published Works:

"Dynamic Rupture Simulations of a Normal Fault in a Heterogeneous Medium", 2009 SSA Annual Meeting, Poster
"Earthquake Ground Motion for the Salt Lake City Segment of the Wasatch Fault", 2009 AGU Fall Meeting, Poster
"Wasatch Fault: Salt Lake City Segment Ground-Motion Simulation", 2010 SSA Annual Meeting, Oral Presentation
"Comparison of Proxies for the 'Velocity Strengthening' Zone at Shallow Depth and Their Effect on Rupture Dynamics", 2010 SCEC Annual Meeting, Poster
"Nucleation by Dynamic Triggering on a Multi-Segment Fault", 2010 AGU Fall Meeting, Oral Presentation